

PerSense: Personalized Instance Segmentation in Dense Images

Muhammad Ibraheem Siddiqui Muhammad Umer Sheikh Hassan Abid Muhammad Haris Khan
Mohamed Bin Zayed University of Artificial Intelligence
Abu Dhabi, UAE

muhammad.siddiqui@mbzuai.ac.ae

Abstract

The emergence of foundational models has significantly advanced segmentation approaches. However, existing models still face challenges in automatically segmenting personalized instances in dense scenarios, where severe occlusions, scale variations, and background clutter hinder precise instance delineation. To address this, we propose **PerSense**, an end-to-end, training-free, and model-agnostic one-shot framework for **Personalized instance Segmentation in dense images**. We start with developing a new baseline capable of automatically generating instance-level point prompts via proposing a novel Instance Detection Module (IDM) that leverages density maps, encapsulating spatial distribution of objects in an image. To reduce false positives, we design the Point Prompt Selection Module (PPSM), which refines the output of IDM based on an adaptive threshold. Both IDM and PPSM seamlessly integrate into our model-agnostic framework. Furthermore, we introduce a feedback mechanism which enables PerSense to improve the accuracy of density maps by automating the exemplar selection process for density map generation. Finally, to promote algorithmic advances and effective tools for this relatively underexplored task, we introduce PerSense-D, an evaluation benchmark exclusive to personalized instance segmentation in dense images. Our extensive experiments establish PerSense superiority in dense scenarios compared to SOTA approaches. Additionally, our qualitative findings demonstrate the adaptability of our framework to images captured in-the-wild. Code: <https://github.com/Muhammad-Ibraheem-Siddiqui/PerSense>

1. Introduction

Imagine working in a food processing sector where the goal is to automate the quality control process for vegetables, such as potatoes, using vision sensors. The challenge is to segment all potato instances in densely packed environments, where variations in scale, occlusions, and background clutter add complexity to the task. We refer to this

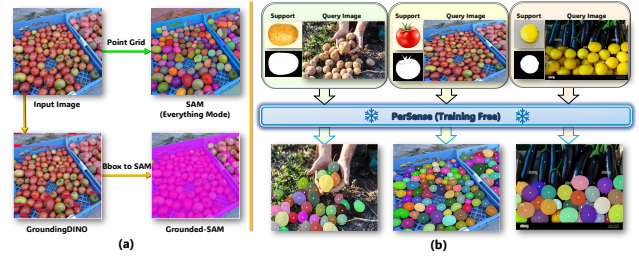


Figure 1. (a) Depicts the deteriorated segmentation performance of Grounded-SAM in dense scenarios and SAM’s ”everything mode” which indiscriminately segments both foreground and background without category personalization. (b) Introducing PerSense, an end-to-end, training-free and model-agnostic one-shot framework for personalized instance segmentation in dense images.

task as *personalized instance segmentation in dense images*, building on the concept of personalized segmentation, first introduced in [1]. The term *personalized* refers to the segmentation of a specific visual category / concept within an image. Our task setting focuses on personalized instance segmentation, particularly in *dense scenarios*.

A natural approach to address this problem is leveraging state-of-the-art (SOTA) foundation models. One key contribution is Segment Anything Model (SAM) [2], which introduces a prompt-driven segmentation framework. However, SAM lacks the ability to segment distinct visual concepts [1]. Its ”everything mode” uses a point grid to segment all objects, including both foreground and background (Fig. 1). Alternatively, users can provide manual prompts to isolate specific instances, making the process labor-intensive, time-consuming, and impractical for large-scale automation. One approach to automation is using box prompts from a pre-trained object detector to isolate the object of interest. Grounded-SAM [3] follows this strategy by forwarding bounding boxes from GroundingDINO [4] to SAM [2] for segmentation. However, bounding boxes are limited by box shape, occlusions, and the orientation of objects [5]. A standard axis-aligned box for a particular object may include portions of adjacent instances. Additionally,

when using non-max suppression (NMS), bounding box-based detections may group closely positioned instances of the same object together. Although techniques like bipartite matching introduced in DETR [6] can address the NMS issue, bounding box-based detections are still challenged due to variations in object scale, occlusions, and background clutter. These challenges become even more pronounced in dense scenes [7], making precise instance segmentation increasingly difficult (Fig. 1).

Point-based prompting, mostly based on manual user input, is generally better than box-based prompting for tasks that require high accuracy, fine-grained control, and the ability to handle occlusions, clutter, and dense instances [8]. However, the automated generation of point prompts using low-shot data, for personalized segmentation in dense scenarios, has largely remained unexplored. Recent works, such as SegGPT [9], PerSAM [1] and Matcher [10], introduce frameworks for one-shot personalized segmentation. Despite their effectiveness in sparsely populated scenes with clearly delineated objects, these methods show limited performance in dense scenarios.

We approach this problem by exploring density estimation methods, which utilize density maps (DMs) to capture the spatial distribution of objects in dense scenes. While DMs effectively estimate global object counts, they struggle with precise instance-level localization [11]. To this end, we introduce *PerSense*, an end-to-end, training-free and model-agnostic one-shot framework (Fig. 1), wherein we first develop a new baseline capable of autonomously generating instance-level candidate point prompts via a proposed Instance Detection Module (IDM), which exploits DMs for precise localization. We generate DMs using a density map generator (DMG) which highlights spatial distribution of object of interest based on input exemplars. To allow automatic selection of effective exemplars for DMG, we automate the process via a class-label extractor (CLE) and a grounding detector. Second, we design a Point Prompt Selection Module (PPSM) to mitigate false positives within the candidate point prompts. Both IDM and PPSM are plug-and-play components, seamlessly integrating into *PerSense*. Lastly, we introduce a robust feedback mechanism, which automatically refines the initial exemplar selection by identifying multiple rich exemplars for DMG based on the initial segmentation output of *PerSense*. This ability to segment personalized concepts in dense scenarios can be pivotal for industrial automation, which uses vision-based sensors for applications such as quality control, and cargo monitoring. Extensive experiments validate *PerSense*'s superiority in both performance and efficiency for dense scenarios, outperforming SOTA methods.

Finally, to our knowledge, no benchmark specifically targets segmentation in dense images. While mainstream datasets like COCO[12], LVIS[13], and FSS-1000 [14] con-

tain images with multiple instances of the same object, they do not represent dense scenarios due to their limited object count. For example, images in the LVIS dataset contain an average of 11.2 instances across 3.4 object categories (3.3 instances per category), which is insufficient to represent dense scenarios. To bridge this gap, we introduce *PerSense-D*, a personalized one-shot evaluation benchmark designed exclusively for segmentation in dense images. *PerSense-D* consists of 717 images across 28 diverse object categories, with an *average of 53 object instances per image*. It includes dot annotations and ground truth masks, featuring images with significant occlusion and background clutter, making it a unique and challenging benchmark for advancing algorithmic development and practical tools in dense environments. Beyond class-wise division, it also provides density-based categorization for fine-grained evaluation.

2. Related Work

One-shot personalized segmentation: As discussed in Sec. 1, SAM [2] lacks semantic awareness, limiting its ability to segment personalized visual concepts. To address this, PerSAM [1] introduces a training-free, one-shot segmentation framework using SAM, effectively segmenting multiple instances of the same category through an iterative masking approach. However, when applying PerSAM to dense images with many instances of the same object, several challenges may arise. (1) Its iterative masking becomes computationally expensive as the number of iterations scales with object count. (2) Confidence map accuracy degrades as more objects are masked, making it harder to distinguish overlapping instances. (3) PerSAM's confidence thresholding strategy which halts the process when the confidence score drops below a set threshold, may lead to premature termination of segmentation process, even when valid objects are still present. In contrast, *PerSense* leverages DMs to generate precise instance-level point prompts in a single pass, eliminating the need for iterative masking and thereby improving segmentation efficiency in dense scenes. Another one-shot segmentation method, SLiMe [15], enables personalized segmentation based on segmentation granularity in the support set, rather than object category. Despite its strong performance, SLiMe tends to produce noisy segmentations for small objects due to the smaller attention maps extracted from Stable Diffusion [16] compared to the input image.

Painter [17] introduces a unified vision model with in-context prompting, eliminating the need for downstream fine-tuning. However, its reliance on masked image modeling prioritizes coarse global features, limiting its ability to capture fine-grained details and handle dense scene complexity. SegGPT [9] builds on Painter by introducing a random coloring approach for in-context training, improving generalization across segmentation tasks. How-

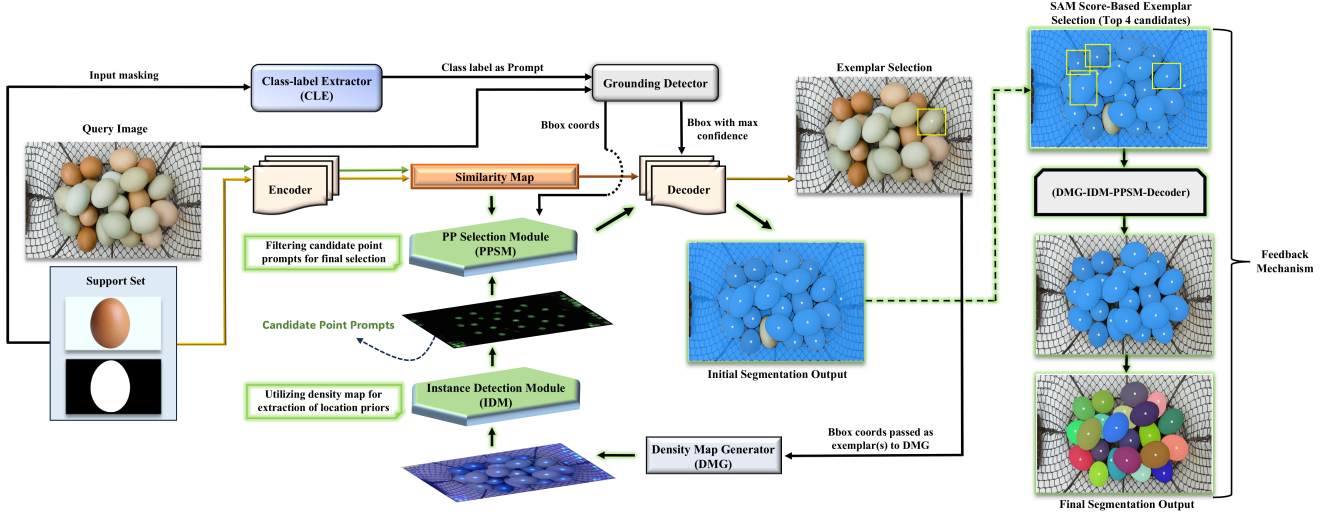


Figure 2. Overall architecture of our PerSense: an *end-to-end*, *training-free* and *model-agnostic one-shot* framework.

ever, in one-shot settings, this scheme may oversimplify densely packed regions, making it difficult to distinguish overlapping objects. Matcher [10] integrates a feature extraction model with a class-agnostic segmentation model, using bidirectional matching for semantic alignment. However, its instance-level matching is limited, impacting instance segmentation performance. Matcher relies on reverse matching to remove outliers and K-means clustering for instance sampling, which can become a bottleneck in dense scenes due to varying object scales. In contrast, PerSense leverages DMG to generate personalized DMs, eliminating the need for clustering and sampling. Additionally, Matcher forwards the bounding box of the matched region as a box prompt to SAM, which inherits limitations of box-based detections, particularly in dense environments.

Interactive segmentation: Recently, interactive segmentation has gained attention, with models like InterFormer [18], MIS [19], and SEEM [20] offering user-friendly interfaces but relying on manual input from the user, which limits scalability. More recently, SemanticSAM [21] improves upon vanilla SAM by incorporating semantic-awareness and multi-granularity segmentation, however it still requires manual prompts and does not explicitly generalize from one-shot reference to all instances of the same category within the image. In contrast, PerSense automates instance-specific point prompt generation from one-shot data, enabling personalized segmentation without manual intervention.

3. Method

We introduce PerSense, a training-free and model-agnostic one-shot framework designed for personalized instance segmentation in dense images (Fig. 2). In following sections,

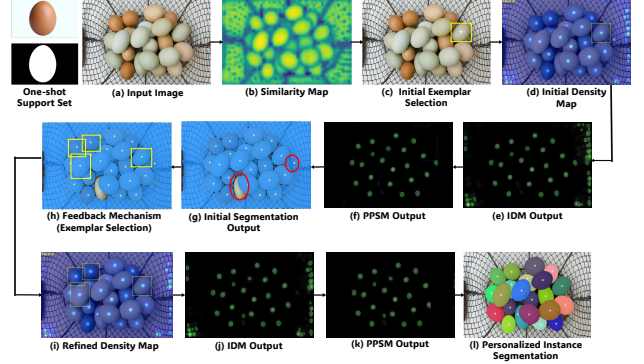


Figure 3. Step-by-step workflow of PerSense components. From an input image (a), a cosine similarity map (b) is generated using the support set. Exemplar selection (c), guided by similarity scores and grounding detector output, produces an initial density map (DM) (d) via DMG. The IDM processes this DM to generate candidate point prompts (e), which are refined by PPSM (f) to filter false positives. The decoder then produces an initial segmentation output (g), where PPSM effectively eliminates false positives; however, a few still remain alongside false negatives (red circle). The feedback mechanism (h) refines exemplar selection based on SAM scores, generating an improved DM (i). IDM and PPSM leverage this refined DM to generate precise point prompts (j, k), leading to personalized instance segmentation (l).

we detail the core components of our PerSense framework. The step-by-step working of PerSense components is depicted in Fig. 3. See Appendix for pseudo-codes.

3.1. Class-label Extraction and Exemplar Selection

PerSense operates as a one-shot framework, leveraging a support set to guide personalized segmentation in a query image based on semantic similarity with the support ob-

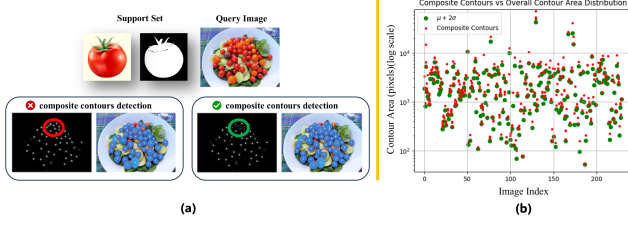


Figure 4. (a) Without identifying composite contours, multiple object instances may be incorrectly grouped (red circle). Identification of composite contours (green circle) enables accurate localization of child contours. (b) The plot illustrates the presence of composite contours beyond $\mu + 2\sigma$ in the contour area distribution for 250 dense images. (best viewed in zoom)

ject. First, input masking is applied to the support image using a coarse support mask to isolate the object of interest. The masked image is then processed by the CLE with the prompt, "Name the object in the image?". The CLE generates a description, from which the noun is extracted as the object category. This category serves as a prompt for the grounding detector, enabling personalized object detection in the query image. To refine the prompt, the term "all" is prefixed to the class label. Next, we compute the cosine similarity score S_{score} between query Q and support S_{supp} features, extracted by the encoder:

$$S_{score}(Q, S_{supp}) = \cos_sim(f(Q), f(S_{support})), \quad (1)$$

where $f(\cdot)$ represents the encoder. Utilizing this score along with detections from the grounding detector, we extract the positive location prior. Specifically, we identify the bounding box B_{max} with the highest detection confidence and proceed to locate the pixel-precise point P_{max} with the maximum similarity score within this bounding box:

$$P_{max} = \arg \max_{P \in B_{max}} S_{score}(P, S_{supp}), \quad (2)$$

where P represents candidate points within the bounding box B_{max} . This identified point serves as the positive location prior, which is subsequently fed to the decoder for segmentation. Additionally, we extract the bounding box surrounding the segmentation mask of the object. This bounding box is then forwarded as an exemplar to the DMG for generation of DM.

3.2. Instance Detection Module (IDM)

The IDM begins by converting the DM from the DMG into a grayscale image I_{gray} . A binary image I_{binary} is created from I_{gray} using a pixel-level threshold T ($T \in [0, 255]$):

$$I_{binary}(x, y) = \begin{cases} 1 & \text{if } I_{gray}(x, y) \geq T \\ 0 & \text{if } I_{gray}(x, y) < T \end{cases} \quad (3)$$

A morphological erosion operation is then applied to I_{binary} using a 3×3 kernel K :

$$I_{eroded}(x, y) = \min_{(i,j) \in K} I_{binary}(x + i, y + j), \quad (4)$$

where I_{eroded} is the eroded image, and (i, j) iterates over the kernel K to refine the boundaries and eliminate noise from the binary image. We deliberately used a small kernel to avoid damaging the original densities of true positives.

Next, contours are extracted from I_{eroded} , and their areas $A_{contour}$ are modeled as a Gaussian distribution:

$$A_{contour} \sim \mathcal{N}(\mu, \sigma^2) \quad (5)$$

where μ represents the mean contour area, corresponding to the typical object size, and σ denotes the standard deviation, capturing variations in contour areas due to differences in object sizes among instances. The mean and standard deviation are computed as:

$$\mu = \frac{1}{N} \sum_{i=1}^N A_i, \quad \sigma = \sqrt{\frac{1}{N} \sum_{i=1}^N (A_i - \mu)^2} \quad (6)$$

where N is the number of detected contours. Composite contours, which encapsulate multiple objects within a single contour, are identified using a threshold $T_{composite}$, defined as $\mu + 2\sigma$ based on the contour size distribution (Fig. 4). These regions, though rare, are detected as outliers exceeding $T_{composite}$. The probability of a contour being composite is given by:

$$P(A_{contour} > T_{composite}) = 1 - \Phi\left(\frac{T_{composite} - \mu}{\sigma}\right) \quad (7)$$

where Φ is the cumulative distribution function (CDF) of the standard normal distribution. For each composite contour, a distance transform $D_{transform}$ is applied to reveal internal sub-regions representing individual object instances:

$$D_{transform}(x, y) = \min_{(i,j) \in B} \|(x, y) - (i, j)\| \quad (8)$$

where B represents contour boundary pixels and (x, y) are the coordinates of each pixel within the region of interest. A binary threshold applied to $D_{transform}$ segments sub-regions within each composite contour, enabling separate identification of overlapping objects in dense scenarios. For each detected contour (parent and child), the centroid is calculated using spatial moments:

$$cX = \frac{M_{10}}{M_{00} + \epsilon}, \quad cY = \frac{M_{01}}{M_{00} + \epsilon} \quad (9)$$

where M_{pq} are the spatial moments of the contour, and ϵ is a

small constant to prevent division by zero. These moments are computed as:

$$(M_{00}, M_{10}, M_{01}) = \sum_x \sum_y I(x, y) \cdot (1, x, y) \quad (10)$$

where $I(x, y)$ is the pixel intensity at position (x, y) . These centroids serve as candidate point prompts, accurately marking the locations of individual object instances in dense scenarios. The candidate point prompts are subsequently forwarded to PPSM for final selection.

3.3. Point Prompt Selection Module (PPSM)

The PPSM serves as a critical component in the PerSense pipeline, filtering candidate point prompts before forwarding the selected points to the decoder for segmentation. Each candidate point from IDM is evaluated based on its query-support similarity score, using an adaptive threshold that adjusts dynamically to object density. This ensures a balance between true positive inclusion and false positive elimination in dense scenes. We statistically model the adaptive threshold in PPSM, scaling it based on object count. Assuming similarity score $S(x, y)$ approximate a Gaussian distribution with mean μ and variance σ^2 , we consider the maximum score S_{\max} as the upper bound, representing the most aligned point with the target feature. The adaptive threshold T for point selection is then defined as:

$$T = \frac{S_{\max}}{C/k}, \quad \text{for } C > 1 \quad (11)$$

where C and k represent the object count and normalization constant, respectively. When $C = 1$, the point associated with S_{\max} is selected as the prompt. As C increases, the threshold T decreases, allowing for a more inclusive selection of points when there is a higher density of objects. We choose $k = \sqrt{2}$, based on empirical results presented in Sec. 5.3. The probability P of a randomly selected point having a similarity score S above T is given by:

$$P(S \geq T) = 1 - \Phi\left(\frac{T - \mu}{\sigma}\right) \quad (12)$$

where Φ is the CDF of the standard normal distribution. Substituting for T , we get:

$$P(S \geq T) = 1 - \Phi\left(\frac{\frac{S_{\max}}{C/k} - \mu}{\sigma}\right) \quad (13)$$

As C increases, the probability of points surpassing the threshold also increases, allowing more candidate points to qualify when object counts are high. Dynamically adjusting T prevents the unintended exclusion of true positives, a common issue when using fixed thresholds aimed strictly at rejecting false positives. This flexibility is crucial, as query-support similarity scores vary significantly, even with minor

intra-class differences. In highly dense images ($C > 50$), the scores for positive location priors can vary widely, necessitating a density-aware adaptive threshold. As object instances increase, intra-class variation becomes more pronounced, further widening the score distribution.

3.4. Feedback Mechanism

PerSense proposes a feedback mechanism to enhance the exemplar selection process for the DMG by leveraging the initial segmentation mask (M_{seg}) from the decoder and the corresponding SAM-generated mask scores (S_{mask}).

$$C_{Top} = \text{Top}_k(M_{seg}, S_{mask}, k), \quad (14)$$

where C_{Top} represents the set of the top k candidates, selected based on their mask scores. In our case $k = 4$ (see Sec. 5.3). These selected candidates are then forwarded as exemplars to DMG in a feedback manner. This leads to improved accuracy of the DM leading to enhanced segmentation performance. The quantitative analysis of this aspect is further discussed in Sec. 5, which explicitly highlights the value added by the proposed feedback mechanism.

4. New Evaluation Benchmark (PerSense-D)

Existing segmentation datasets like COCO [12], LVIS [13], and FSS-1000 [14] contain multi-instance images, but most do not represent dense scenarios due to limited object counts. For instance, images in LVIS average 11.2 instances across 3.4 categories, yielding only 3.3 instances per category. To bridge this gap, we introduce PerSense-D, a diverse segmentation benchmark designed exclusively for dense scenarios. *It contains 717 images across 28 object categories, averaging 53 object instances per image.* PerSense-D serves as a challenging benchmark to drive algorithmic advancements and support practical applications across domains such as agriculture, environmental monitoring, and autonomous systems.

Image Collection and Retrieval: Out of 717 images, we have 689 dense query images and 28 support images. To acquire the set of 689 dense images, we initiated the process with a collection of candidate images obtained through keyword searches. To mitigate bias, we retrieved the candidate images by querying object keywords across three distinct Internet search engines: Google, Bing, and Yahoo. To diversify the search query keywords, we prefixed adjectives such as 'multiple', 'lots of', and 'many' before the category names. In every search, we collected the first 100 images. With 28 categories, we gathered a total of 2800 images, which were subsequently filtered in the next step.

Manual Inspection and Filtering: The candidate images were manually inspected following a three-point criterion. (1) The image quality and resolution should be sufficiently high to enable easy differentiation between objects. (2) Fol-

Method	Venue	Density-based (mIoU)			Class-wise (mIoU)
		Low	Med	High	Overall
<i>End-to-end trained / fine-tuned</i>					
C3Det [29]	CVPR 2022	52.70	46.64	39.11	48.60
SegGPT [9]	ICCV 2023	59.81	53.34	52.05	55.50
PerSAM-F [†] [1]	ICLR 2024	38.18	34.84	26.73	29.30
PseCo [†] [30]	CVPR 2024	53.99	65.23	68.55	61.83
GeCo [†] [31]	NIPS 2024	63.92	63.40	74.49	65.95
<i>Training-free</i>					
PerSAM [†] [1]	ICLR 2024	32.27	28.75	20.25	24.45
TFOC [†] [32]	WACV 2024	<u>62.78</u>	65.38	65.69	62.63
Matcher [†] [10]	ICLR 2024	58.62	58.30	68.00	62.80
GroundedSAM [†] [3]	arXiv 2024	58.36	66.24	64.97	65.92
PerSense [†] (DMG1)	(ours)	66.36	67.27	74.78	70.96
PerSense [†] (DMG2)	(ours)	59.84	73.51	77.57	71.61

Table 1. Comparison of PerSense with SOTA segmentation approaches on PerSense-D benchmark. We report density-based evaluation along with class-wise performance following the evaluation protocol in Section 4. [†] indicates method using SAM.

Method	Venue	COCO-20 ⁱ					LVIS-92 ⁱ
		F0	F1	F2	F3	Mean mIoU	Mean mIoU
<i>In-domain training</i>							
HSNet [33]	CVPR 21	37.2	44.1	42.4	41.3	41.2	17.4
VAT [34]	ECCV 22	39.0	43.8	42.6	39.7	41.3	18.5
FPTrans [35]	NIPS 22	44.4	48.9	50.6	44.0	47.0	-
MIANet [36]	CVPR 23	42.4	52.9	47.7	47.4	47.6	-
LLaFS [37]	CVPR 24	47.5	58.8	56.2	53.0	53.9	-
<i>COCO as training data</i>							
Painter [17]	CVPR 23	31.2	35.3	33.5	32.4	33.1	10.5
SegGPT [9]	ICCV 23	56.3	57.4	58.9	51.7	56.1	18.6
<i>Training-free (excluding PerSAM-F [1])</i>							
PerSAM [†] [1]	ICLR 24	23.1	23.6	22.0	23.4	23.0	11.5
PerSAM-F [†] [1]	ICLR 24	22.3	24.0	23.4	24.1	23.5	12.3
Matcher [†] [10]	ICLR 24	52.7	53.5	52.6	52.1	52.7	33.0
PerSense[†]	(ours)	<u>47.8</u>	<u>49.3</u>	48.9	<u>50.1</u>	<u>49.0</u>	<u>25.7</u>

Table 2. Comparison of PerSense with SOTA approaches on COCO-20ⁱ and LVIS-92ⁱ. [†] indicates method using SAM.

dence matrix struggles to identify distinct regions when there is significant overlap or occlusion among objects. To be fair in comparison with Grounded-SAM, we ensured that all classes in PerSense-D overlap with the datasets used for GroundingDINO pretraining (notably, all classes are present in Objects365 dataset [28]). PerSense surpassed Grounded-SAM by **+5.69%**, demonstrating its robustness.

Since object counting methods primarily target dense scenes, we compare PerSense with the recently introduced training-free object counting framework (TFOC) [32], which formulates the counting task as a segmentation problem. PerSense outperforms TFOC by **+8.98%**. Additionally, we evaluate PerSense against SOTA counting approaches PseCo [30] and GeCo [31] which essentially are dense object detectors end-to-end trained on FSC-147 dataset. PerSense outperforms PseCo by **+9.78%** and GeCo by **+5.66%**, demonstrating its superiority. Finally, we com-

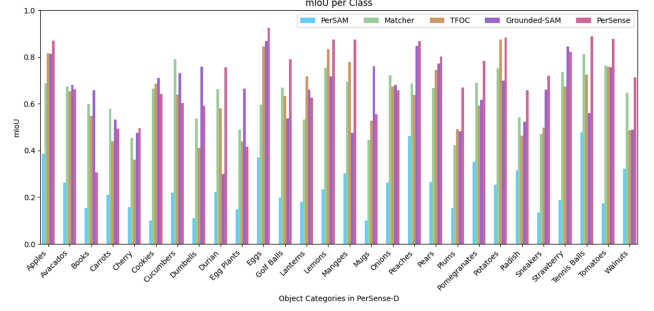


Figure 7. Class-wise mIoU comparison between PerSense and SOTA training-free approaches on the PerSense-D benchmark.

pare PerSense with C3Det [29], a multi-class tiny object detector trained on Tiny-DOTA dataset [38]. Using the positive location prior from PerSense as the initial user input, C3Det was tasked to detect similar instances, which were then segmented using SAM. PerSense outperformed C3Det by **+23.01%**. We present a class-wise comparison of PerSense with SOTA training-free approaches in Fig. 7. Meanwhile, Fig. 8 presents qualitative comparison with SOTA, and Fig. 9 demonstrates *in-the-wild* performance.

For a fine-grained analysis, we additionally evaluate PerSense’s segmentation performance across varying object densities, following the PerSense-D density-based categorization discussed in Sec. 4. We compute mIoU separately for low, medium, and high-density images, where PerSense outperforms all methods, establishing itself as the SOTA for personalized segmentation in dense images. An interesting observation is the monotonic increase in PerSense’s segmentation performance from low to high density images. This is due to DMs generated by DMG, which are inherently suited for structured object distributions in dense environments. In low-density images, object sparsity limits high-confidence regions, making point prompt generation challenging. As density increases, the DM becomes richer, enabling IDM to extract more precise points, thereby improving segmentation accuracy in denser scenarios.

Performance on Sparse Benchmarks: PerSense is specifically designed for dense images, deriving point prompts from DMs generated by DMG. As a result, it is naturally not expected to give SOTA performance on sparse benchmarks with few object instances, e.g. LVIS averages 3.3 instances per category. For images with single or low object count, DM tends to spread across the entire object, reducing its effectiveness and undermining its primary purpose of capturing variations in object density across the image. In such cases, traditional object detection methods are more effective due to fewer occlusions and easier object boundary delineation, rendering DM generation inefficient. Nonetheless, to provide a comprehensive evaluation, we evaluate PerSense on COCO-20ⁱ [39] and LVIS-

(a)			(b)				(c)		(d)		(e)				
Method	Memory (MB)	Avg Inf time (sec)	Modules	baseline (mIoU)	baseline + PPSM (mIoU)	PerSense (mIoU)	Norm Factor	mIoU	No. of Exemplars	mIoU	No. of Iterations	1	2	3	4
Grounded-SAM [3]	2943	1.8	IDM	yes	yes	yes	1	70.41	1	65.78	PerSense (mIoU)	70.96	70.97	70.96	70.95
PerSAM [1]	2950	($C \times 1.02$)	PPSM	no	yes	yes	$\sqrt{2}$	70.96	2	69.24					
Matcher [10]	3209	10.2	Feedback	no	no	yes	$\sqrt{3}$	69.59	3	70.53					
PerSense (this work)	2988	2.7					$\sqrt{5}$	68.95	4	70.96	Avg Inf time (sec)	2.7	3.1	3.5	3.9
			PerSense-D (Gain)	65.58 (-)	66.95 (+1.37)	70.96 (+4.01)			5	70.90					
			COCO (Gain)	46.33 (-)	48.81 (+2.48)	49.00 (+0.19)			6	70.81					

Table 3. (a) Running efficiency comparison of PerSense with SOTA (C represents instance count). (b) Component-wise ablation study of PerSense. (c) Choice of normalization factor for adaptive threshold in PPSM. (d) Varying number of exemplars in DMG using feedback mechanism. (e) Impact of multiple feedback iterations on PerSense performance.

92ⁱ [13], demonstrating that despite being tailored for dense scenes, PerSense maintains competitive performance even in sparse settings. To provide a broader perspective, we compare PerSense with both in-domain training methods and training-free approaches (Table 2). Despite being a training-free framework, PerSense achieves performance comparable to several well-known in-domain training methods. PerSense demonstrates significant improvements over PerSAM-F, achieving mIoU gains of **+25.5%** on COCO-20ⁱ and **+13.4%** on LVIS-92ⁱ. PerSense outperforms SegGPT [9] on LVIS-92ⁱ by **+7.1%**. However, SegGPT demonstrates superior performance on COCO-20ⁱ, as it is included in its training set. Additionally, PerSense surpasses Painter [17] on COCO-20ⁱ and LVIS-92ⁱ by **+15.9%** and **+15.2%** mIoU, respectively, despite Painter being trained on COCO. Overall, PerSense ranks second-best among SOTA, trailing only Matcher [10]. This highlights PerSense robustness and generalization ability, even in scenarios outside its primary design focus.

Runtime Efficiency: Table 3a provides inference time and memory consumption details for PerSense, evaluated on a single NVIDIA GeForce RTX 4090 GPU (batch size = 1). PerSense is computationally efficient than Matcher and PerSAM and incurs marginal latency and GPU memory usage compared to Grounded-SAM, though with a trade-off in segmentation accuracy.

Limitations: While PerSense employs IDM and PPSM to refine DMs and reject false positives, respectively, it cannot recover any true positives missed initially by DMG, during DM generation. Figure 10 illustrates this limitation.

5.3. Ablation Study

Component-wise Ablation: The PerSense framework comprises three key components: IDM, PPSM, and a feedback mechanism. An ablation study presented in Table 3b quantifies their respective contributions. Integrating PPSM into our baseline network improved mIoU by **+1.37%** on PerSense-D and **+2.48%** on COCO, effectively mitigating false positives in IDM-generated point prompts. The feedback mechanism further increased mIoU by **+4.01%** on PerSense-D, demonstrating its effectiveness in optimizing exemplar selection. However, its impact on COCO was lim-

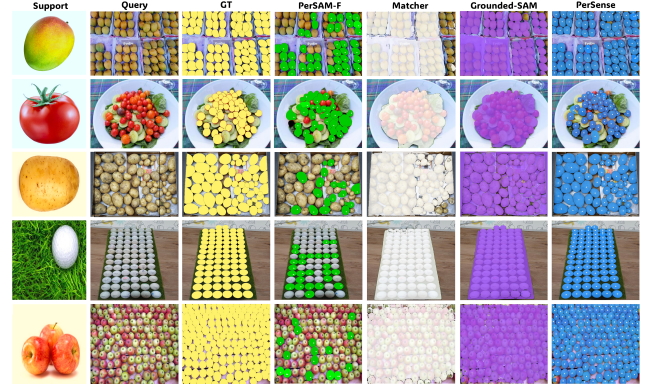


Figure 8. Qualitative comparison of PerSense with SOTA.



Figure 9. PerSense *in-the-wild*. 1st row: Input, 2nd row: Output.

ited (**+0.19%**) due to insufficient object instances, restricting its ability to refine the DM.

Choice of Normalization Factor in PPSM: For the PPSM adaptive threshold, we initialized the normalization constant at 1 and applied a square root progression for a gradual step-size increase. Empirical results show that $\sqrt{2}$ yields the most significant mIoU improvement (Table 3c).

Varying No. of Exemplars in Feedback Mechanism: We automated the selection of the best exemplars for DMG based on SAM scores using the proposed feedback mechanism. As shown in Table 3d, segmentation performance on PerSense-D saturates after four exemplars, as additional exemplars do not provide any new significant information about the object of interest.

Multiple Iterations in Feedback Mechanism: The PerSense feedback mechanism refines the DM in a single pass by selecting exemplars from the initial segmentation

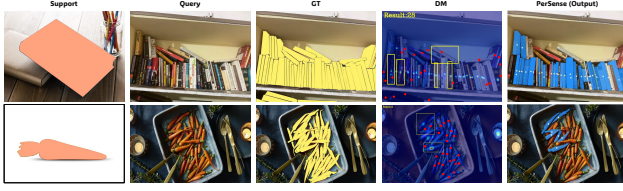


Figure 10. The figure illustrates scenarios where PerSense’s performance deteriorates, primarily due to its reliance on the generated density map. In the first row, where the goal is to segment all instances of the “book” class, the density map excludes many true positives (highlighted in red), which PerSense cannot recover once they are lost during DM generation. A similar issue is seen in the second row, where a poor-quality density map for the “carrot” class leads to missed instances, negatively impacting PerSense segmentation performance.

output based on SAM scores. We analyzed multiple iterations (Table 3e) and found no accuracy gains but increased computational overhead. This occurs because first-pass exemplars, with well-defined boundaries, are already effectively captured by SAM. Subsequent iterations redundantly select the same exemplars due to their distinct features and consistently high SAM scores.

6. Conclusion

We presented PerSense, a training-free and model-agnostic one-shot framework for personalized instance segmentation in dense images. We proposed IDM and PPSM, which transforms DMs from DMG into personalized instance-level point prompts for segmentation. We also proposed a robust feedback mechanism in PerSense which automates and improves the exemplar selection process in DMG. Finally to promote algorithmic advancements considering the persense task, we introduced PerSense-D, a benchmark exclusive to dense images. We established superiority of our method in dense scenarios by comparing it with the SOTA.

References

- [1] R. Zhang, Z. Jiang, Z. Guo, S. Yan, J. Pan, H. Dong, P. Gao, and H. Li, “Personalize segment anything model with one shot,” *The Twelfth International Conference on Learning Representations*, 2024. 1, 2, 6, 7, 8
- [2] A. Kirillov, E. Mintun, N. Ravi, H. Mao, C. Rolland, L. Gustafson, T. Xiao, S. Whitehead, A. C. Berg, W.-Y. Lo *et al.*, “Segment anything,” in *Proceedings of the IEEE/CVF International Conference on Computer Vision*, 2023, pp. 4015–4026. 1, 2, 6
- [3] T. Ren, S. Liu, A. Zeng, J. Lin, K. Li, H. Cao, J. Chen, X. Huang, Y. Chen, F. Yan *et al.*, “Grounded sam: Assembling open-world models for diverse visual tasks,” *arXiv preprint arXiv:2401.14159*, 2024. 1, 7, 8
- [4] S. Liu, Z. Zeng, T. Ren, F. Li, H. Zhang, J. Yang, C. Li, J. Yang, H. Su, J. Zhu *et al.*, “Grounding dino: Marrying dino with grounded pre-training for open-set object detection,” *arXiv preprint arXiv:2303.05499*, 2023. 1, 6
- [5] M. Zand, A. Etemad, and M. Greenspan, “Oriented bounding boxes for small and freely rotated objects,” *IEEE Transactions on Geoscience and Remote Sensing*, vol. 60, pp. 1–15, 2021. 1
- [6] N. Carion, F. Massa, G. Synnaeve, N. Usunier, A. Kirillov, and S. Zagoruyko, “End-to-end object detection with transformers,” in *European conference on computer vision*. Springer, 2020, pp. 213–229. 2
- [7] J. Wan and A. Chan, “Adaptive density map generation for crowd counting,” in *Proceedings of the IEEE/CVF international conference on computer vision*, 2019, pp. 1130–1139. 2
- [8] K.-K. Maninis, S. Caelles, J. Pont-Tuset, and L. Van Gool, “Deep extreme cut: From extreme points to object segmentation,” in *Proceedings of the IEEE conference on computer vision and pattern recognition*, 2018, pp. 616–625. 2
- [9] X. Wang, X. Zhang, Y. Cao, W. Wang, C. Shen, and T. Huang, “Seggpt: Towards segmenting everything in context,” in *Proceedings of the IEEE/CVF International Conference on Computer Vision*, 2023, pp. 1130–1140. 2, 6, 7, 8
- [10] Y. Liu, M. Zhu, H. Li, H. Chen, X. Wang, and C. Shen, “Matcher: Segment anything with one shot using all-purpose feature matching,” in *The Twelfth International Conference on Learning Representations*, 2024. 2, 3, 6, 7, 8
- [11] J. Pelhan, V. Zavrtanik, M. Kristan *et al.*, “Dave-a detect-and-verify paradigm for low-shot counting,” in *Proceedings of the IEEE/CVF Conference on Computer Vision and Pattern Recognition*, 2024, pp. 23 293–23 302. 2
- [12] T.-Y. Lin, M. Maire, S. Belongie, J. Hays, P. Perona, D. Ramanan, P. Dollár, and C. L. Zitnick, “Microsoft coco: Common objects in context,” in *Computer Vision–ECCV 2014: 13th European Conference, Zurich, Switzerland, September 6–12, 2014, Proceedings, Part V 13*. Springer, 2014, pp. 740–755. 2, 5, 6
- [13] A. Gupta, P. Dollar, and R. Girshick, “Lvis: A dataset for large vocabulary instance segmentation,” in *Proceedings of the IEEE/CVF conference on computer vision and pattern recognition*, 2019, pp. 5356–5364. 2, 5, 6, 8
- [14] X. Li, T. Wei, Y. P. Chen, Y.-W. Tai, and C.-K. Tang, “Fss-1000: A 1000-class dataset for few-shot segmentation,” in *Proceedings of the IEEE/CVF conference on computer vision and pattern recognition*, 2020, pp. 2869–2878. 2, 5
- [15] A. Khani, S. Asgari, A. Sanghi, A. M. Amiri, and G. Hamarneh, “Slime: Segment like me,” in *The Twelfth International Conference on Learning Representations*, 2023. 2
- [16] R. Rombach, A. Blattmann, D. Lorenz, P. Esser, and B. Ommer, “High-resolution image synthesis with latent diffusion models,” in *Proceedings of the IEEE/CVF conference on computer vision and pattern recognition*, 2022, pp. 10 684–10 695. 2
- [17] X. Wang, W. Wang, Y. Cao, C. Shen, and T. Huang, “Images speak in images: A generalist painter for in-context visual learning,” in *Proceedings of the IEEE/CVF Conference on*

- Computer Vision and Pattern Recognition*, 2023, pp. 6830–6839. 2, 7, 8
- [18] Y. Huang, H. Yang, K. Sun, S. Zhang, L. Cao, G. Jiang, and R. Ji, “Interformer: Real-time interactive image segmentation,” in *Proceedings of the IEEE/CVF International Conference on Computer Vision (ICCV)*, October 2023, pp. 22 301–22 311. 3
 - [19] K. Li, Y. Zhao, Z. Wang, Z. Cheng, P. Jin, X. Ji, L. Yuan, C. Liu, and J. Chen, “Multi-granularity interaction simulation for unsupervised interactive segmentation,” in *Proceedings of the IEEE/CVF International Conference on Computer Vision (ICCV)*, October 2023, pp. 666–676. 3
 - [20] X. Zou, J. Yang, H. Zhang, F. Li, L. Li, J. Wang, L. Wang, J. Gao, and Y. J. Lee, “Segment everything everywhere all at once,” *Advances in Neural Information Processing Systems*, vol. 36, 2024. 3
 - [21] F. Li, H. Zhang, P. Sun, X. Zou, S. Liu, C. Li, J. Yang, L. Zhang, and J. Gao, “Segment and recognize anything at any granularity,” in *European Conference on Computer Vision*. Springer, 2024, pp. 467–484. 3
 - [22] V. Ranjan, U. Sharma, T. Nguyen, and M. Hoai, “Learning to count everything,” in *Proceedings of the IEEE/CVF Conference on Computer Vision and Pattern Recognition*, 2021, pp. 3394–3403. 6
 - [23] M. Cai, H. Liu, S. K. Mustikovela, G. P. Meyer, Y. Chai, D. Park, and Y. J. Lee, “Making large multimodal models understand arbitrary visual prompts,” in *Proceedings of the IEEE conference on computer vision and pattern recognition*, 2024. 6
 - [24] A. Radford, J. W. Kim, C. Hallacy, A. Ramesh, G. Goh, S. Agarwal, G. Sastry, A. Askell, P. Mishkin, J. Clark *et al.*, “Learning transferable visual models from natural language supervision,” in *International conference on machine learning*. PMLR, 2021, pp. 8748–8763. 6
 - [25] W.-L. Chiang, Z. Li, Z. Lin, Y. Sheng, Z. Wu, H. Zhang, L. Zheng, S. Zhuang, Y. Zhuang, J. E. Gonzalez *et al.*, “Vicuna: An open-source chatbot impressing gpt-4 with 90%* chatgpt quality,” See <https://vicuna.lmsys.org> (accessed 14 April 2023), vol. 2, no. 3, p. 6, 2023. 6
 - [26] J. He, B. Liu, F. Cao, J. Xu, and Y. Xiao, “Few-shot object counting with dynamic similarity-aware in latent space,” *IEEE Transactions on Geoscience and Remote Sensing*, 2024. 6
 - [27] C. Liu, Y. Zhong, A. Zisserman, W. Xie, and C. M. I. Center, “Countr: Transformer-based generalised visual counting,” 2022. 6
 - [28] S. Shao, Z. Li, T. Zhang, C. Peng, G. Yu, X. Zhang, J. Li, and J. Sun, “Objects365: A large-scale, high-quality dataset for object detection,” in *Proceedings of the IEEE/CVF international conference on computer vision*, 2019, pp. 8430–8439. 7
 - [29] C. Lee, S. Park, H. Song, J. Ryu, S. Kim, H. Kim, S. Pereira, and D. Yoo, “Interactive multi-class tiny-object detection,” in *Proceedings of the IEEE/CVF Conference on Computer Vision and Pattern Recognition*, 2022, pp. 14 136–14 145. 7
 - [30] Z. Huang, M. Dai, Y. Zhang, J. Zhang, and H. Shan, “Point segment and count: A generalized framework for object counting,” in *Proceedings of the IEEE/CVF Conference on Computer Vision and Pattern Recognition*, 2024, pp. 17 067–17 076. 7
 - [31] J. Pelhan, A. Lukezic, V. Zavrtanik, and M. Kristan, “A novel unified architecture for low-shot counting by detection and segmentation,” in *The Thirty-eighth Annual Conference on Neural Information Processing Systems*. 7
 - [32] Z. Shi, Y. Sun, and M. Zhang, “Training-free object counting with prompts,” in *Proceedings of the IEEE/CVF Winter Conference on Applications of Computer Vision*, 2024, pp. 323–331. 7
 - [33] J. Min, D. Kang, and M. Cho, “Hypercorrelation squeeze for few-shot segmentation,” in *Proceedings of the IEEE/CVF international conference on computer vision*, 2021, pp. 6941–6952. 7
 - [34] S. Hong, S. Cho, J. Nam, S. Lin, and S. Kim, “Cost aggregation with 4d convolutional swin transformer for few-shot segmentation,” in *European Conference on Computer Vision*. Springer, 2022, pp. 108–126. 7
 - [35] J.-W. Zhang, Y. Sun, Y. Yang, and W. Chen, “Feature-proxy transformer for few-shot segmentation,” *Advances in neural information processing systems*, vol. 35, pp. 6575–6588, 2022. 7
 - [36] Y. Yang, Q. Chen, Y. Feng, and T. Huang, “Mianet: Aggregating unbiased instance and general information for few-shot semantic segmentation,” in *Proceedings of the IEEE/CVF Conference on Computer Vision and Pattern Recognition*, 2023, pp. 7131–7140. 7
 - [37] L. Zhu, T. Chen, D. Ji, J. Ye, and J. Liu, “Llafs: When large language models meet few-shot segmentation,” in *Proceedings of the IEEE/CVF Conference on Computer Vision and Pattern Recognition*, 2024, pp. 3065–3075. 7
 - [38] G.-S. Xia, X. Bai, J. Ding, Z. Zhu, S. Belongie, J. Luo, M. Datcu, M. Pelillo, and L. Zhang, “Dota: A large-scale dataset for object detection in aerial images,” in *Proceedings of the IEEE conference on computer vision and pattern recognition*, 2018, pp. 3974–3983. 7
 - [39] K. Nguyen and S. Todorovic, “Feature weighting and boosting for few-shot segmentation,” in *Proceedings of the IEEE/CVF International Conference on Computer Vision*, 2019, pp. 622–631. 7

Appendix

Algorithm 1: PerSense

Input: Query Image (I_Q), Support Image (I_S), Support Mask (M_S)

Output: Segmentation Mask

- 1 Perform input masking: $I_{\text{masked}} = I_S \odot M_S$;
 - 2 Extract class-label using CLE from I_{masked} (text prompt: "Name the object in the image?");
 - 3 Prompt grounding detector with class-label;
 - 4 Obtain grounded detections;
 - 5 Bounding box with max confidence \rightarrow decoder;
 - 6 Obtain segmentation mask of the object;
 - 7 Refine bounding box coordinates using the segmentation mask;
 - 8 Exemplar Selection: Refined bounding box \rightarrow DMG;
 - 9 Obtain DM from DMG;
 - 10 Process DM using IDM to generate candidate point prompts (PP_{cand});
 - 11 $PP_{\text{cand}} \rightarrow$ PPSM \rightarrow final point prompts (PP_{final});
 - 12 $PP_{\text{final}} \rightarrow$ decoder;
 - 13 Obtain an initial segmentation output;
 - 14 Select Top 4 candidates as DMG exemplars based on SAM score;
 - 15 Feedback: Repeat Steps 8 to 13;
 - 16 Obtain final segmentation output;
-

Algorithm 2: Instance Detection Module (IDM)

Input: Density Map (DM) from DMG

Output: Candidate Point Prompts (PP)

- 1 Convert DM to grayscale image (I_{gray});
 - 2 Threshold to binary (threshold = 30) to obtain binary image (I_{binary});
 - 3 Erode I_{binary} using 3×3 kernel;
 - 4 Find BLOB.contours (C_{BLOB}) in the eroded image (I_{eroded});
 - 5 **for** contour in C_{BLOB} **do**
 - 6 Compute contour area (A_{contour});
 - 7 Find center pixel coordinates for each contour;
 - 8 **end**
 - 9 Compute mean (μ) and standard deviation (σ) using A_{contour} ;
 - 10 Detect composite.contours ($C_{\text{composite}}$) by thresholding A_{contour} ;
 - 11 $\text{area_threshold} = \mu + 2\sigma$;
 - 12 **for** contour in C_{BLOB} **do**
 - 13 Compute A_{contour} ;
 - 14 **if** $A_{\text{contour}} > \text{area_threshold}$ **then**
 - 15 save contour as $C_{\text{composite}}$;
 - 16 **end**
 - 17 **end**
 - 18 **for** contour in $C_{\text{composite}}$ **do**
 - 19 Apply distance transform [threshold = $0.5 * \text{dist_transform.max}()$];
 - 20 Find child contours;
 - 21 Find center pixel coordinates for each child contour;
 - 22 **end**
 - 23 **return** center points from Steps 7 and 21 as candidate PP;
-

Algorithm 3: Point Prompt Selection Module (PPSM)

Input: candidate_PP, similarity_matrix, object_count, grounded_detections

Output: selected_PP

```
1 max_score ← Get the maximum similarity score from similarity_matrix;
2 selected_PP ← [ ]; // Empty list to store selected_PP
3 sim_threshold ← max_score / (object_count /  $\sqrt{2}$ );
4 for each PP in candidate_PP do
5   PP_similarity ← similarity_matrix(PP);
6   for each box in grounded_detections do
7     if (PP_similarity > sim_threshold) and (PP lies within box) then
8       selected_PP.append(PP);
9     end
10  end
11 end
12 return selected_PP;
```
